ARTICLE

Characterization of Sol−Gel-Encapsulated Proteins Using Small-Angle Neutron Scattering

Guangming Luo,[†,‡] Qiu Zhang,[†,§] Alexis Rae Del Castillo,[†,⊥] Volker Urban,[*,†] and Hugh O'Neill[*,†]

Center for Structural Molecular Biology and Biodeuteration Laboratory, Chemical Sciences Division, Oak Ridge National Laboratory, Oak Ridge, Tennessee 37831

ABSTRACT Entrapment of biomolecules in silica-derived sol−gels has grown into a vibrant area of research since it was originally demonstrated. However, accessing the consequences of entrapment on biomolecules and the gel structure remains a major challenge in characterizing these biohybrid materials. We present the first demonstration that it is possible with small-angle neutron scattering (SANS) to study the conformation of dilute proteins that are entrapped in transparent and dense sol−gels. Using deuterium-labeled green fluorescent protein (GFP) and SANS with contrast variation, we demonstrate that the scattering signatures of the sol−gel and the protein can be separated. Analysis of the scattering curves of the sol−gels using a mass-fractal model shows that the size of the colloidal silica particles and the fractal dimensions of the gels were similar in the absence and presence of protein, demonstrating that GFP did not influence the reaction pathway for the formation of the gel. The major structural difference in the gels was that the pore size was increased 2-fold in the presence of the protein. At the contrast match point for silica, the scattering signal from GFP inside the gel became distinguishable over a wide q range. Simulated scattering curves representing a monomer, end-to-end dimer, and parallel dimer of the protein were calculated and compared to the experimental data. Our results show that the most likely structure of GFP is that of an end-to-end dimer. This approach can be readily applied and holds great potential for the structural characterization of complex biohybrid and other materials.

KEYWORDS: sol−gel • enzyme • protein entrapment • small-angle neutron scattering • protein conformation

INTRODUCTION

Proteins entrapped in an open pore network structure such as silica sol−gels are of technological interest for potential applications such as bioconversion, drug delivery, and biosensors (1−3). In addition, sol−gel chemistry can be used as an analytical tool for biophysical studies of protein dynamics and function (3). In this approach, the biomolecule is encapsulated in a silica matrix obtained through hydrolysis and polycondensation of an alkoxide precursor [usually tetramethyl (TMOS) or tetraethyl orthosilicate], yielding a porous structure that allows rapid exchange of solutes between the gel matrix and the surrounding medium (1). The structural and dynamic properties of the entrapped protein can be examined by assay of enzyme function and also various spectroscopic measurements. The latter include techniques such as UV−visible (2), circular dichroism (4), fluorescence (5), resonance Raman (6), and nuclear magnetic resonance (7). However, direct evaluation of the consequences of entrapment on the biomolecule structure remains a major challenge. In this study, the structure of green fluorescent protein (GFP) entrapped in sol−gels was investigated using small-angle neutron scattering (SANS). Using deuterium labeling and phase-contrast variation, we demonstrate that it is possible to separate the scattering signatures of the protein and the sol−gel.

GFP and its homologues are used for a wide range of applications in cellular and molecular biology (8, 9). Crystallographic studies reveal a protein with a β-barrel structure and a central chromophore that is formed by autocatalytic cyclization and oxidation of residues serine 65, tyrosine 66, and glycine 67 (10). GFP has very high fluorescence emission, which allows detection at the single-molecule level (11), and a subset of GFP mutants have recently been described that undergo light-induced transitions between distinct nonfluorescent and fluorescent ground states (12). Such reversibly switchable fluorescent proteins have been proposed for bioelectronic applications such as high-density optical memories and photonic switches (12−14). An important factor in realizing this goal is the ability to achieve high spatial resolution of the protein in the device architecture and knowledge of the distribution and aggregation of the protein in gels.

The direct investigation of an entrapped protein's conformation, structure, and aggregation state would be advantageous for this application and many other studies. However, these measurements are hindered because of interference from the sol−gel matrix. One recent study demonstrated that NMR may be used to acquire atomic level structural

* E-mail: oneillhm@ornl.gov (H.O'N.), urbanvs@ornl.gov (V.U.).
Received for review June 20, 2009 and accepted September 23, 2009
† Center for Structural Molecular Biology.
‡ Present address: Chemical Science and Engineering Division, Argonne National Laboratory, 9700 S. Cass Avenue, Argonne, IL 60439.
§ Biodeuteration Laboratory.
⊥ Presently employed in industry.
DOI: 10.1021/am900430v

Published on Web 10/08/2009

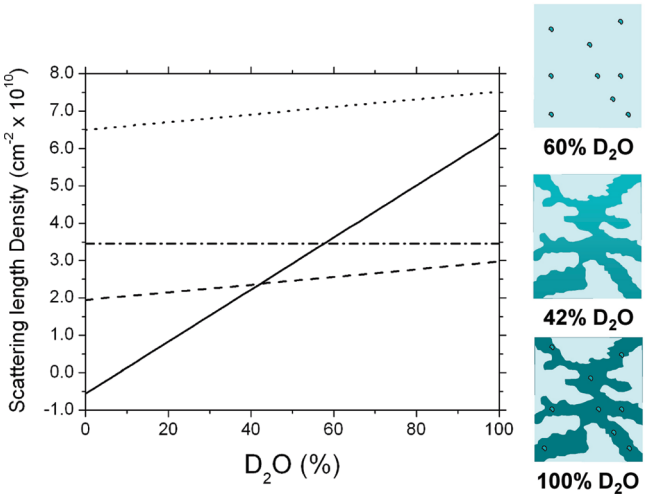

FIGURE 1. Variation in the SLD of water and solutes at different ratios of H_2O/D_2O: water (—); hydrogenated protein (- - -); SiO_2 (— · —); deuterated protein (· · ·). A pictorial representation of the phase-contrast variation technique is shown on the right. Hydrogenated protein is depicted as small disks, the silica gel is in light blue, and the solvent "color" varies with the D_2O concentration. A detailed explanation is provided in the text.

detail of proteins entrapped in sol—gels (7). For characterization of the nanostructure of these inorganic—organic hybrid materials, small angle scattering techniques, using X-rays (15) and neutrons (16), are very important because they provide structural information over many length scales (1.0—100 nm) and are nondestructive techniques. The same techniques can also be used to provide structural information about the size and shape of proteins and protein complexes in solution (17). Neutrons, in particular, have an added advantage over X-rays and light because different isotopes scatter neutrons very differently. Figure 1 shows how the scattering length density (SLD) of water can be modulated over a wide range from a negative value ($\rho_{H_2O} = -0.56 \times 10^{10}$ cm^{-2}) to a positive value ($\rho_{D_2O} = 6.4 \times 10^{10}$ cm^{-2}) by varying the hydrogen-to-deuterium ratio (18). In a multicomponent system, the SLD of individual components can be selectively matched to the solvent, allowing the scattering signal of other components to be observed. For example, silica can be matched at approximately 60% D_2O (19), allowing the signature of protein to be observed, hydrogenated protein can be matched at 42% D_2O, and at other concentrations of D_2O, all components contribute to the scattering profile. It is important to note that, as shown in Figure 1, the SLD of fully deuterated protein is greater than 100% D_2O and therefore its scattering contribution cannot be matched to the solvent. In the present investigation, the SLD of deuterated protein was used to provide maximum contrast for the dilute protein at the match point for silica gel and solvent. One previous study attempted to deconvolute the SANS signal of entrapped protein and the silica gel matrix but was unsuccessful because of technical issues related to scattering from the sol—gel matrix (20). Earlier work by Vidal et al. focused on protein crystallization in the presence of dilute silica gel [approximately 1% (w/v)] and drew conclusions on the partition of the protein lysozyme between the solution and the gel surface but did not extract size and shape information of the individual protein molecules (19).

MATERIALS AND METHODS

Overexpression and Purification of Deuterated GFP. GFP was overexpressed in *Escherichia coli* BL21 (DE3) cells transformed with the plasmid pAcGFP1 that encodes the gene for *Aequorea coerulescens* GFP (BD Biosciences, San Jose, CA) using standard techniques. Enfors (21) minimal medium, with 0.5% (w/v) glycerol-d_8 as the carbon source, was used for the production of deuterated protein, as described previously (22). A modified three-phase partitioning approach (23) was carried out as the first step in the purification procedure. This step was followed by purification by anion-exchange chromatography (AEC) on a 5 mL Hi-trap Q FF column (GE Healthcare) using a salt gradient from 50 mM Tris/HCl pH 8.0 (buffer A) to 50 mM Tris/HCl pH 8.0 and 1 M NaCl (buffer B) over 15 column volumes. The concentration of GFP was determined using $\epsilon_{492\ nm} = 33.5$ mM^{-1} cm^{-1}, and its purity was determined by sodium dodecyl sulfate—polyacrylamide gel electrophoresis (SDS-PAGE) analysis. All measurements were performed using deuterated GFP, unless otherwise noted.

Sol—Gel Synthesis. A total of 0.01 mol of tetramethyl orthosilicate (TMOS) was mixed with 0.338 g of H_2O and 0.02 g of 40 mM HCl, and the resulting solution was sonicated at 4 °C until a homogeneous solution was formed (approximately 20 min). GFP dissolved in a 30 mM Tris buffer, pH 8.0, was mixed with the sol solution in a volume ratio of 2:3, to a final concentration of 2.7 mg mL^{-1}. A control gel was also synthesized under the same conditions except that protein was not added. After gelation occurred, the gels were overlaid with H_2O, which was replaced several times over a 24 h period. They were then incubated in the D_2O solutions for 48 h with three changes of solution to ensure that all exchangeable hydrogen atoms were exchanged to deuterium.

Analysis Methods. Circular dichroism (CD) spectra were recorded on a Jasco 810 CD spectropolarimeter from 190 to 600 nm at 25 °C. The fluorescence spectra were recorded on a fluorescence monochromator (FMO-427S/427 L) attachment on the CD instrument. UV—visible spectra were recorded between 190 and 800 nm using a Cary 50 spectrophotometer.

SANS Measurements. Gels were placed in 1 × 1 × 4.5 cm quartz cuvettes together with a small amount of H_2O/D_2O solvent to maintain a humidified environment and minimize dehydration of the gels. SANS measurements of protein solutions were conducted in a 100% D_2O buffer in 2-mm-path-length quartz cells.

SANS experiments were carried out using the CG-2 and CG-3 beamlines at the High Flux Isotope Reactor in Oak Ridge National Laboratory (24). Sol—gel data were recorded at CG-2 for scattering vectors $0.009 < q < 0.19$ Å^{-1} (where $q = (4\pi/\lambda)\sin(\theta/2)$, λ is the neutron wavelength, and θ is the scattering angle) using neutrons of wavelength $\lambda = 4.75$ Å ± 15% and a 1 m × 1 m, position-sensitive He^3 area detector, placed at 5.8 m distance from the sample and offset 0.25 m from the direct beam axis. Solution samples were measured on the CG-3 Bio-SANS instrument ($\lambda = 6$ Å ± 15%) with a 0.4 m × 0.4 m, position-sensitive He^3 detector at a 1.1 m sample-to-detector distance, offset 0.2 m. The recorded scattering intensities were normalized to the accumulated transmitted neutron flux and irradiated sample volume and corrected for detector response efficiency and background. The circular scattering patterns were then azimuthally averaged and normalized to intensity per solid scattering angle. Dilute solution data were further corrected for scattering from the solvent.

Analysis of SANS Data from Sol—Gels. The SANS scattering data from sol—gels was modeled as described by Teixeira (25).

The experimentally observed scattering intensity from the system can be given as

$$I(q) = ANP(q)\,S(q) + B \tag{1}$$

A is a scale factor, which depends on the instrument parameters and sample dimensions, N is the number density of scattering particles, and B is the experimental background. $P(q)$ is the form factor of the primary particle, e.g.

$$P(q) = V^2(\rho - \rho_0)^2\{3[\sin(qR_0) - qR_0\cos(qR_0)]/(qR_0)^3\}^2 \tag{2}$$

for a spherical particle with volume V and radius R_0. The contrast term $(\rho - \rho_0)^2$ is the square of the difference between the scattering length densities of the particle and solvent. $S(q)$ describes the dependence of the scattered intensity on interparticle interaction, which in the present case leads to the arrangement of primary particles into a fractal structure

$$S(q) = 1 + \frac{\sin[(d-1)\tan^{-1}(q\xi)]}{(qR_0)^d}\,\frac{d\Gamma(d-1)}{[1 + 1/(q^2\xi^2)]^{(d-1)/2}} \tag{3}$$

d is the fractal dimension, and ξ is the cutoff distance for the self-similarity and is interpreted as the pore size in the gels, as described previously (26). SANS curves with different neutron scattering contrasts between the gel and solvent were obtained by varying the D_2O concentration. A simultaneous fit of curves with different scattering length contrasts was used to yield an average result with higher statistical confidence. During the fit, the intensity scale factor and background, which depend on the D_2O concentration, were allowed to vary for each curve, while the structural parameters R_0, d, and ξ were forced to be identical for all three curves [0, 30, and 100% (v/v) D_2O].

Analysis of GFP in Sol–Gels. A SANS curve of GFP can be derived from its pair distribution function:

$$I(q) = A \times 4\pi \int \mathrm{d}r\, P(r)\,\frac{\sin(qr)}{qr} + B \tag{4}$$

$P(r)$ is the pair distribution function of the protein. If the protein's atomic structure is known, then

$$P(r) = \sum_{i,j} f(\mathbf{r}_i)\,f(\mathbf{r}_j)\,\delta(|\mathbf{r}_i - \mathbf{r}_j| - r) \tag{5}$$

where $f(r)$ is the excess scattering length of an atom at position r. The crystal structure of *Aequorea victoria* GFP (27) (PDB accession number 1GFL) was used for the simulation.

RESULTS

Our overall aim was to investigate the structural properties of GFP entrapped in silica gel. Perdeuterated *A. coerulescens* recombinant GFP was used in this study to provide maximum contrast between the protein and the solvent during phase-contrast variation experiments. The recombinant GFP was overexpressed in *E. coli* grown in D_2O-based broth (21) with deuterated glycerol as the carbon source. It was purified from the crude cell extract by a combination of three-phase partitioning (23) and AEC. Analysis by PAGE revealed the presence of a single band, indicating that the purified GFP was free of contaminating proteins (Figure 2a; lane 2). Partially and fully denatured proteins are shown for comparison (Figure 2a; lanes 3 and 4).

The sol–gels were synthesized by acid-catalyzed hydrolysis of the sol–gel precursor followed by a condensation reaction at near neutral pH, allowing entrapment of the protein as the gelation reaction proceeded (2). This approach produced transparent and dense vitreous materials. The UV–visible, fluorescence emission, and far-UV–CD spectra of *A. coerulescens* GFP are shown in Figure 2. Encapsulation does not induce any appreciable changes in the properties of the protein. The absorption maxima are in the same position in the UV–visible spectra of the solution and gel samples (Figure 2b), and the elevated baseline in the gel sample is due to scattering from the silica matrix. In the fluorescence emission spectra, the peak was blue-shifted by approximately 2 nm, suggesting that the environment sensed by the protein may be slightly different after entrapment (Figure 2c). A similar observation was reported for GFP entrapped in a polyacrylamide matrix (14). The secondary structures of the free and entrapped proteins were very similar, both exhibiting a minimum at 215 nm that is indicative of the characteristic β-sheet conformation of GFP (5), giving good confidence that the structural integrity of the protein remains intact after encapsulation (Figure 2d).

For SANS experiments, the gels were cast as single contiguous structures 1 mm in thickness and subsequently divided into four equal portions for equilibration in 0, 30, 60, and 100% (v/v) D_2O to ensure structural uniformity between samples. The mass composition was $Si(OH)_4$:water:GFP = 1:1.93:0.008. A set of control gels without protein were prepared in the same manner. Parts a and b of Figure 3 show a log–log plot of the SANS data for gels in 100, 30, and 0% (v/v) D_2O. The contrast in the wet gel originates from the differences in the SLD of the solvent and that of the silica network. The intensity of scattering decreased monotonously over the range of scattering vectors, q. Previous SANS investigations (26, 28) have used a mass fractal model described by Teixeira (25) to describe the morphology of sol–gels in terms of spherical silica primary particles that aggregate into larger clusters, which, in turn, pack randomly, forming a porous cluster network. The arrangement of primary particles with radius R_0 into clusters follows mass fractal behavior with fractal dimension d and cutoff distance ξ of the fractal correlation. A simultaneous fit of our SANS spectra with different concentrations of D_2O (100, 30, and 0%) shows that R_0 is 13.73 ± 0.1 Å, the fractal dimension, d, is 2.5, and ξ, which characterizes the pore size (28) in the gels, is 33.69 ± 0.11 Å (Figure 3a). In the presence of protein, R_0 is similar (12.24 ± 0.08 Å), while the pore size increased ($\xi = 66.01 \pm 0.27$ Å) and is accompanied by a slight change of the fractal dimension to 2.3 (Figure 3b).

The SANS spectra of control and GFP gels at 100% and 60% D_2O are shown in Figure 3c. The scattering signal is

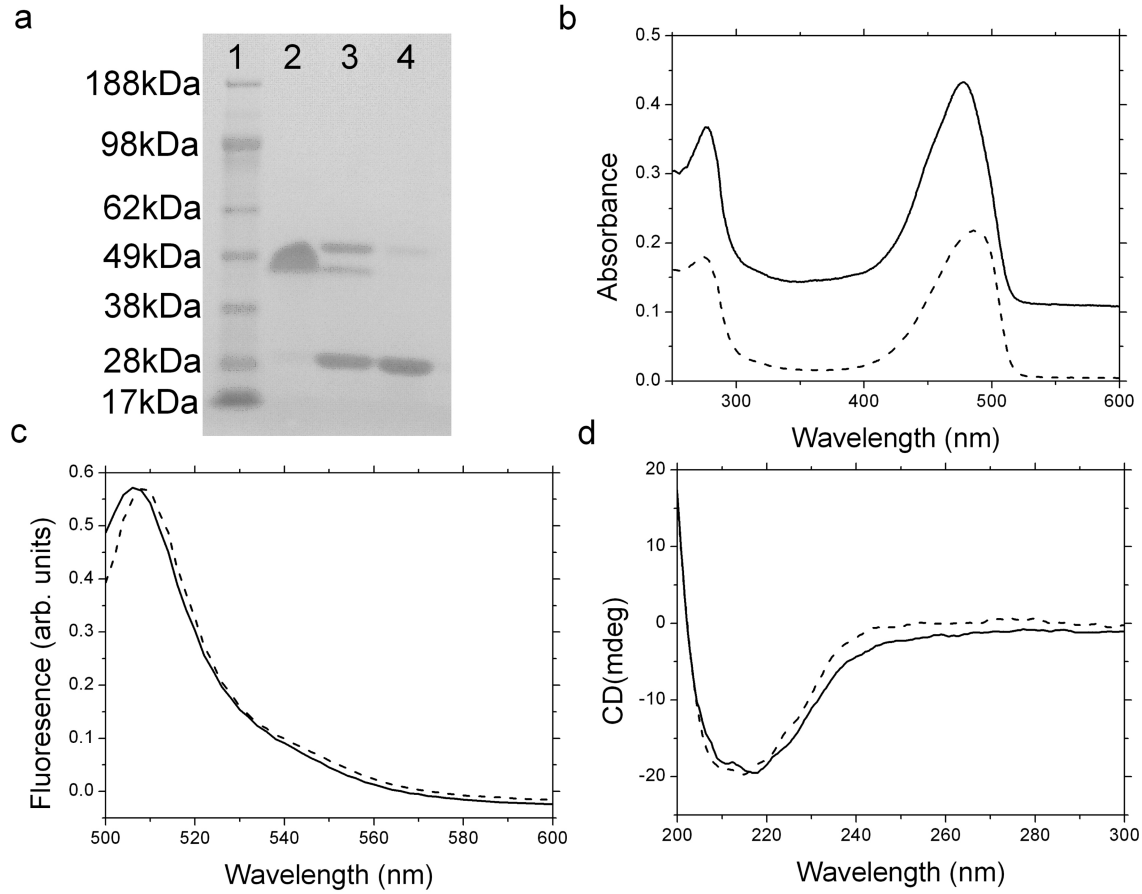

FIGURE 2. Comparison of the physiochemical properties of *A. coerulescens* GFP in solution and entrapped in sol−gels. (a) SDS-PAGE analysis. Lane 1: molecular mass markers. Lane 2: GFP, not denatured. Lane 3: GFP denatured at 70 °C. Lane 4: GFP denatured at >95 °C. (b−d) Comparison of UV−visible spectra, fluorescence emission, and CD spectra of GFP in solution (dashed line) and entrapped in sol−gels (solid line).

strongly reduced at 60% D_2O, indicating that the signal from the silica gel is very weak, as expected in the vicinity of the silica contrast match point. The intensity levels off to a flat plateau at about $q > 0.05$ Å^{-1}, where the scattering is dominated by incoherent H_2O scattering. A plot of the square root of the scattering intensity in the control gels versus the volume fraction of D_2O revealed that the contrast match point for the silica matrix was 62 ± 1.7%, indicating that we are practically at the contrast match point for silica. This value for the sol−gel contrast match point is in agreement with previously published values (19, 29) (Figure S1 in the Supporting Information). The scattering signals from the GFP-containing gel and its control at 100% D_2O are nearly identical at $q > 0.03$ Å^{-1} but differ at $q < 0.03$ Å^{-1}, which is described in the model by a larger value of ξ in the GFP gel, as stated above.

Because of the virtual extinction of the silica scattering in the 60% D_2O data, the signal from GFP inside the gel becomes distinguishable over a wide q range. The scattering curve for GFP was extracted by subtracting the residual silica scattering measured in the control sample at 60% D_2O. This procedure provides a good approximation at the higher q values, where the gels with and without protein scatter similarly, but will fail at $q < 0.03$ Å^{-1} because of the observed differences in the gel scattering. The GFP scattering curve contains information about the overall shape and conformation of the entrapped biomolecule. With knowledge of the crystal structure of the protein, it is possible to simulate its scattering curve and compare it to the experimental data. Because the crystal structure for *A. coerulescens* GFP is not available, the structure for *A. victoria* GFP (27) was used to simulate the scattering curves. This protein shares 92% sequence identity with *A. victoria* GFP and is therefore expected to have a very similar structure (30). In the first instance, a simulated curve representing a protein monomer was fitted to the data because it was previously reported that this is the preferred state of *A. coerulescens* GFP (30). The result is shown in Figure 4a and clearly shows that the curve does not fit the data well ($\chi^2 = 20.38$). PAGE analysis of *A. coerulescens* GFP (Figure 1a, lane 2) strongly suggested that it is present as a dimer in solution, whereas the fully denatured protein migrates in the gel with a mass consistent with the known mass of the polypeptide chain (Figure 2a, lane 4). A fit of the data with a simulated scattering curve representing a parallel or side-by-side dimer indicated that a more extended structure was required to describe the experimental scattering curve ($\chi^2 = 5.92$), Therefore, a scattering curve representing an end-to-end dimer was calculated and compared to the experimental data. Again, the results are shown in Figure 3 and unambiguously demonstrate that the end-to-end dimer ($\chi^2 = 1.11$) is a better model than the side-by-side dimer ($\chi^2 = 5.92$).

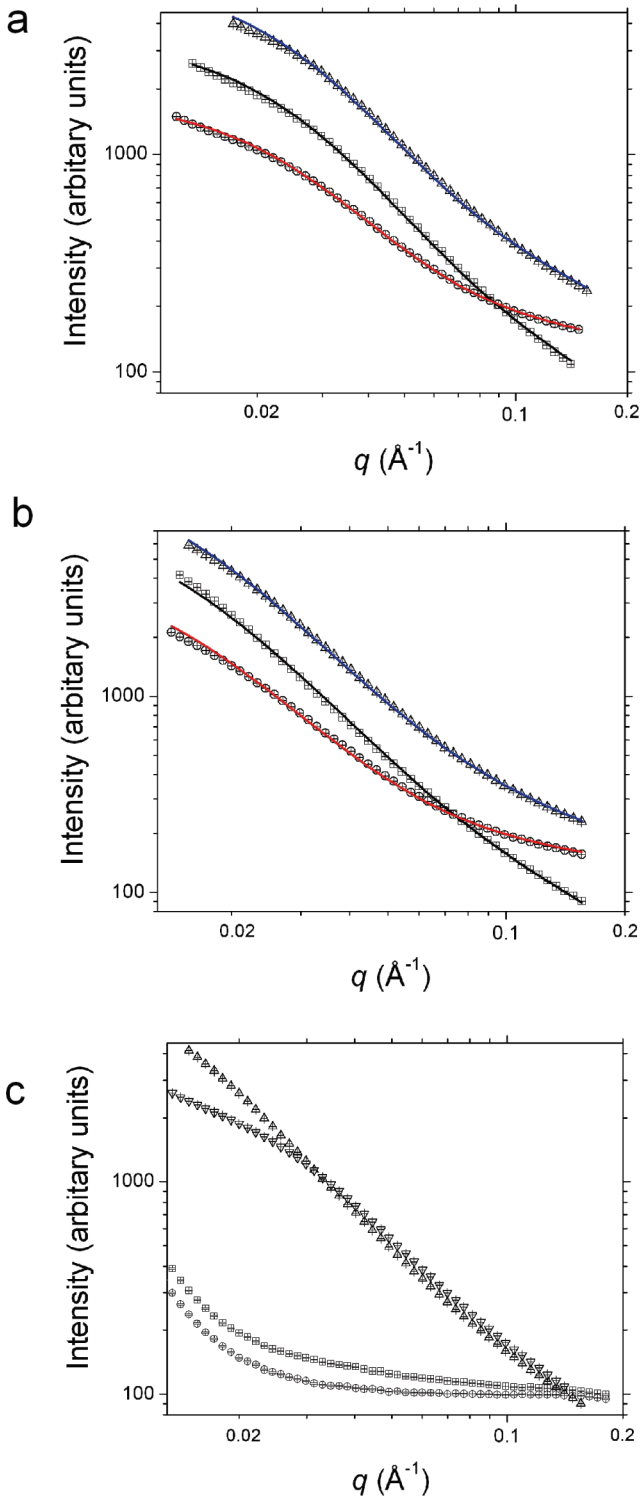

FIGURE 3. SANS spectra of the protein and control silica gels. (a) Control gels: 100% D_2O (⊞), 30% D_2O (⊕), and 0% D_2O (⍋). (b) Protein gels: 100% D_2O (⊞), 30% D_2O (⊕), and 0% D_2O (⍋). In panels a and b, the curves from the mass fractal fitting routine are shown as blue (0% D_2O), red (30% D_2O), and black (100% D_2O) lines. (c) Protein gel in 100% D_2O (⍋), protein gel in 60% D_2O (⊞), control gel in 100% D_2O (⍒), and control gel in 60% D_2O (⊕).

The simulated scattering curves for the three GFP oligomerization states were also fit with the experimental data for hydrogenated GFP in a D_2O solution, measured for comparison with the data obtained from the deuterated protein entrapped in the sol–gel. The scattering curve fits well to an end-to-end dimer, while the more compact models of a monomer or even a parallel dimer do not show satisfactory agreement with the experimental data (Figure S2 in the Supporting Information). In Figure 4b, the shapes of scattering profiles from hydrogenated GFP in a D_2O buffer and deuterated GFP in gel are compared by rescaling the absolute intensity. The constant background B, obtained from the fit to the GFP model shown in Figure 4a, was subtracted for the scattering profile of deuterated GFP in the gel. As shown in Figure 4b, the curves overlay well, giving good confidence that their structures are similar. This result shows that the preferred state for *A. coerulescens* GFP is as an end-to-end dimer and encapsulation in silica gels does not disrupt its quaternary structure. The mass of the scattering particle was also extracted from the solution scattering data using the absolute scattering intensity I_0 extrapolated to $q = 0$ by Guinier's approximation (31) and comparing it to the I_0 obtained from the scattering profile of a known reference protein measured under identical conditions (see the Supporting Information). *Trichoderma reesi* Cellobiohydrolase I was used as the reference protein, and the value obtained for the mass of *A. coerulescens* GFP from its scattering profile was 57 600 ± 6740 Da. The mass of a single GFP polypeptide chain is 27 159.5 Da based on its amino acid sequence, giving good confidence that it is a dimer at the concentration used in this study.

DISCUSSION

In this study, GFP was entrapped in a sol–gel matrix and SANS was used to simultaneously investigate both the structure of proteins entrapped in sol–gels and the structural properties of the gel matrix. Encapsulation of proteins in sol–gels is typically carried out by a two-step process (2). A sol solution is prepared by acid-catalyzed hydrolysis of TMOS to form reactive monomers, followed by polycondensation of the monomers to form colloidal oligomers. The resulting sol solution is mixed with the protein preparation at neutral pH, driving the condensation of the silica particles to form the sol–gel. The protein becomes entrapped in the growing network of silica particles as the condensation reaction proceeds. Anionic proteins such as GFP are postulated to tumble freely within the pores of the negatively charged silicate matrix, sensing an environment similar to aqueous solution, while cationic proteins such as lysozyme strongly interact with the silicate walls and have restricted rotation in the gels (19, 32, 33). As described in the Introduction, there are only a few physicochemical techniques that are able to probe the structural properties of the encapsulated protein, the majority of which are spectroscopic techniques. The major challenge in directly probing the structure of proteins entrapped in sol–gels is separation of the signature of the protein from that of the surrounding matrix.

This is the first report where SANS was successfully employed to investigate the structural properties of dilute protein molecules confined in a dense, vitreous silica sol–gel. By using SANS with contrast variation, it was possible to simultaneously investigate the structure of proteins entrapped in sol–gels and also the structural properties of the

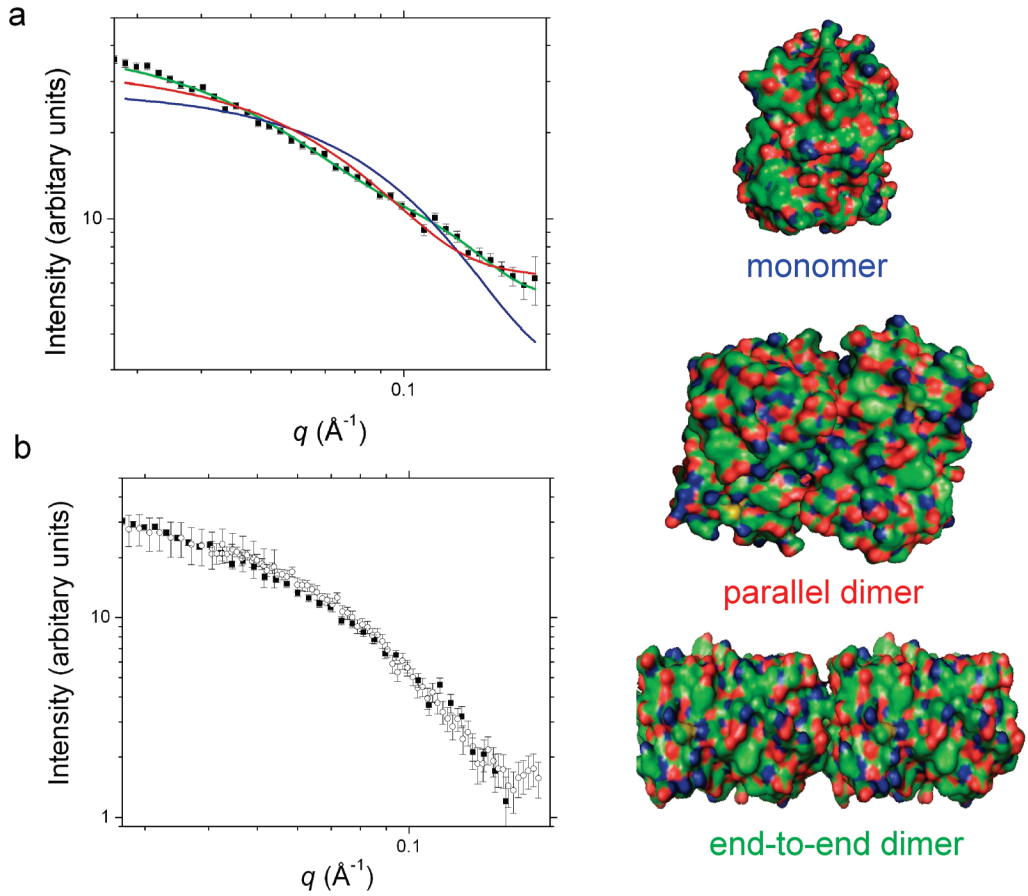

FIGURE 4. Comparison of scattering profiles of GFP in solution and entrapped in sol−gel. (a) Fit of the scattering contribution of GFP entrapped in sol−gel with a theoretical scattering curve of GFP conformations calculated from its crystal structure. The experimental scattering data are shown as solid squares. The simulated scattering curves for a monomer (blue), a parallel dimer (red), and an end-to-end dimer (green) are shown as solid lines. The GFP structures (PDB accession number 1GFL) used for the analysis are also shown. (b) Comparison of the shape of the scattering curve of hydrogenated GFP in solution and deuterated GFP entrapped in sol−gel. The scattering curve for hydrogenated GFP (2.96 mg mL^{-1}) in 10 mM Tris/HCl, pH 7.4, in 100% D_2O is shown as open circles. The scattering curve for deuterated GFP in sol−gel is shown as solid squares.

gel matrix. A fractal model (25) fitted the scattering profiles well, allowing characterization of key features of the sol−gel matrix to be investigated, including the size of the colloidal silica particles, how they interact to form the gel, and also the pore size of the gel. The relatively low concentration of GFP in the gel means that its contribution to the overall scattering profiles of the SANS spectra for 0, 30, and 100% (v/v) D_2O is very low. This allows investigation of changes to the gel structure when GFP is present. The fact that the same structural parameters derived from the simultaneous fitting could be used to fit the curves measured in different concentrations of D_2O demonstrates that the contribution of GFP to the scattering signal is small. The size of colloidal silica particles and the fractal dimension of the gels were similar in the absence and presence of protein, demonstrating that its presence did not influence the reaction pathway for the formation of the gel. Fractal dimensions of less than 3 are considered to be mass fractals, and the observed values of 2.3 and 2.5 indicate that the gel matrix formed by condensation of the silica particles as a branched polymeric network. The major structural difference between the protein and control gels is that the correlation length (ξ), interpreted in this study as the pore size of the gel, increased 2-fold in the presence of protein.

The difference in the SLD of silica and protein was used to selectively highlight the scattering contribution of the protein in the composite material. By using perdeuterated GFP, a protein in which all nonexchangeable protons are exchanged for deuterons, the contrast between the protein (SLD = 7.11×10^{-6} Å^{-2}, in 60% D_2O) and solvent was maximized at the contrast match point for the silica gel (60% D_2O, SLD = 3.62×10^{-6} Å^{-2}). For comparison, the SLD of hydrogenated protein is 2.56×10^{-6} Å^{-2} in 60% D_2O, so it is also feasible to make these measurements with hydrogenated protein but higher concentrations will be required to improve the signal-to-noise ratio. Analysis of the scattering contribution of the protein by a Fourier transform approach made it possible to determine that the most likely conformation of GFP is an end-to-end dimer. Furthermore, it was possible to discriminate between other GFP quaternary structures, indicating that this approach is sensitive to the conformational state of the protein.

NMR spectroscopy has also been used to investigate the structural properties of proteins in sol−gels. Whereas SANS provides structural information to ~1 nm resolution, NMR spectroscopy can provide atomic-level structural detail of proteins in solution with resolutions comparable to those of crystallographic techniques. This approach was successful

in obtaining partial structural information from hydrogenated anionic and neutral porphyrin-containing proteins entrapped in deuterated sol–gels at concentrations ranging from 10 to 16 mg mL^{-1} and analyzed by ^1H NMR (7). Although peaks corresponding to the porphyrin center and surrounding amino acids could be resolved, H_2O and the primary methyl groups of the TMOS precursor present in the sample obscured a large part of the spectrum of the proteins. In addition, the spectrum of horse heart cyctochrome *c*, a cationic protein, was poorly resolved by this approach because electrostatic interactions with the silicate strongly hindered the rotation of protein in the pores. In comparison, SANS is not influenced by these issues and therefore will be able to provide structural information about the conformational state of a wide range of biomolecules entrapped in sol–gels, albeit with lower resolution.

CONCLUSIONS

Analysis of SANS from sol–gel-encapsulated GFP demonstrates that this technique can distinguish the molecular envelope of the entrapped biomolecule. In addition, differences in the structural properties of the sol–gel matrix with and without protein could also be characterized. In principle, our approach does not require deuteration of the protein because the contrast match points for silica and hydrogenated protein are well separated. However, in practice, the versatility of this approach can be increased by using deuterated protein to maximize the contrast between the protein and solvent at the match point of silica, making it possible to investigate a wide range of proteins at relatively low concentrations. Thus, neutron scattering methods hold great potential for the structural characterization of these complex systems, and future exciting applications of this technique will be the development of improved biologically active materials. In addition, it will also find relevance in the investigation of protein folding in crowded environments, visualization of kinetic intermediates during protein–ligand binding studies, and other studies that are not amenable to investigation in dilute solution.

Acknowledgment. We thank Dr. Sai Venkatesh Pingali for assistance with data collection, Dr. Ken Littrell for development of the SANS data reduction software, and Dr. Dean Myles for his support on this project. This research was sponsored by the Laboratory Directed Research and Development Program of Oak Ridge National Laboratory (ORNL) and by the Office of Biological and Environmental Research, using facilities supported by the U.S. Department of Energy (DOE), managed by UT-Battelle, LLC, under Contract DE-AC05-00OR22725. A.R.D.C. was supported by a DOE Science Undergraduate Laboratory Internship managed by Oak Ridge Institute of Science and Education.

Supporting Information Available: Further details on the analysis of SANS data and the approach used to determine the mass of GFP from the scattering data and figures showing the D_2O contrast series for the control sol–gels and the scattering profile of hydrogenated GFP in solution. This material is available free of charge via the Internet at http://pubs.acs.org.

REFERENCES AND NOTES

(1) Braun, S.; Rappoport, S.; Zusman, R.; Avnir, D.; Ottolenghi, M. *Mater. Lett.* **1990**, *10*, 1–5.
(2) Ellerby, L. M.; Nishida, C. R.; Nishida, F.; Yamanaka, S. A.; Dunn, B.; Valentine, J. S.; Zink, J. I. *Science* **1992**, *255*, 1113–1115.
(3) Avnir, D.; Coradin, T.; Lev, O.; Livage, J. *J. Mater. Chem.* **2006**, *16*, 1013–1030.
(4) Eggers, D. K.; Valentine, J. S. *Protein Sci.* **2001**, *10*, 250–261.
(5) Campanini, B.; Bologna, S.; Cannone, F.; Chirico, G.; Mozzarelli, A.; Bettati, S. *Protein Sci.* **2005**, *14*, 1125–1133.
(6) Droghetti, E.; Smulevich, G. *J. Biol. Inorg. Chem.* **2005**, *10*, 696–703.
(7) Wheeler, K. E.; Nocek, J. M.; Hoffman, B. M. *J. Am. Chem. Soc.* **2006**, *128*, 14782–14783.
(8) Stepanenko, O. V.; Verkhusha, V. V.; Kuznetsova, I. M.; Uversky, V. N.; Turoverov, K. K. *Curr. Protein Pept. Sci.* **2008**, *9*, 338–369.
(9) Zimmer, M. *Chem. Rev.* **2002**, *102*, 759–781.
(10) Ormo, M.; Cubitt, A. B.; Kallio, K.; Gross, L. A.; Tsien, R. Y.; Remington, S. J. *Science* **1996**, *273*, 1392–1395.
(11) Cannone, F.; Bologna, S.; Campanini, B.; Diaspro, A.; Bettati, S.; Mozzarelli, A.; Chirico, G. *Biophys. J.* **2005**, *89*, 2033–2045.
(12) Cinelli, R. A. G.; Pellegrini, V.; Ferrari, A.; Faraci, P.; Nifosi, R.; Tyagi, M.; Giacca, M.; Beltram, F. *Appl. Phys. Lett.* **2001**, *79*, 3353–3355.
(13) Stiel, A. C.; Andresen, M.; Bock, H.; Hilbert, M.; Schilde, J.; Schonle, A.; Eggeling, C.; Egner, A.; Hell, S. W.; Jakobs, S. *Biophys. J.* **2008**, *95*, 2989–2997.
(14) Di Benedetto, F.; Biasco, A.; Bizzarri, R.; Arosio, D.; Ricci, F.; Beltram, F.; Cingolani, R.; Pisignano, D. *Langmuir* **2006**, *22*, 29–31.
(15) Peterlik, H.; Fratzl, P. *Monatsh. Chem.* **2006**, *137*, 529–543.
(16) Allen, A. J. *J. Am. Ceram. Soc.* **2005**, *88*, 1367–1381.
(17) Koch, M. H. J.; Vachette, P.; Svergun, D. I. *Q. Rev. Biophys.* **2003**, *36*, 147–227.
(18) May, R. P.; Ibel, K.; Haas, J. *J. Appl. Crystallogr.* **1982**, *15*, 15–19.
(19) Vidal, O.; Robert, M. C.; Boue, F. *J. Cryst. Growth* **1998**, *192*, 271–281.
(20) Rodgers, L. E.; Holden, P. J.; Knott, R. B.; Finnie, K. S.; Bartlett, J. R.; Foster, L. J. R. *J. Sol–Gel Sci. Technol.* **2005**, *33*, 65–69.
(21) Artero, J. B.; Hartlein, M.; McSweeney, S.; Timmins, P. *Acta Crystallogr., Sect. D: Biol. Crystallogr.* **2005**, *61*, 1541–1549.
(22) Weiss, K. L.; Meilleur, F.; Blakeley, M. P.; Myles, D. A. A. *Acta Crystallogr., Sect. F: Struct. Biol. Cryst. Commun.* **2008**, *64*, 537–540.
(23) Jain, S.; Singh, R.; Gupta, M. N. *J. Chromatogr. A* **2004**, *1035*, 83–86.
(24) Lynn, G. W.; Heller, W.; Urban, V.; Wignall, G. D.; Weiss, K.; Myles, D. A. A. *Phys. B* **2006**, *385–86*, 880–882.
(25) Teixeira, J. *J. Appl. Crystallogr.* **1988**, *21*, 781–785.
(26) Lelong, G.; Price, D. L.; Douy, A.; Kline, S.; Brady, J. W.; Saboungi, M. L. *J. Chem. Phys.* **2005**, *122*, 164504.
(27) Yang, F.; Moss, L. G.; Phillips, G. N. *Nat. Biotechnol.* **1996**, *14*, 1246–1251.
(28) Margaca, F. M. A.; Salvado, I. M. M.; Teixeira, J. *J. Non-Cryst. Solids* **1999**, *258*, 70–77.
(29) Lelong, G.; Price, D. L.; Brady, J. W.; Saboungi, M. L. *J. Chem. Phys.* **2007**, *127*, 065102.
(30) Gurskaya, N. G.; Fradkov, A. F.; Pounkova, N. I.; Staroverov, D. B.; Bulina, M. E.; Yanushevich, Y. G.; Labas, Y. A.; Lukyanov, S.; Lukyanov, K. A. *Biochem. J.* **2003**, *373*, 403–408.
(31) Guinier, A.; Fournet, G. *Small-Angle Scattering of X-rays*; Wiley: New York, 1955.
(32) Chirico, G.; Beretta, S.; Cannone, F.; Diaspro, A.; Bettati, S.; Campanini, B.; Mozzarelli, A. *Biophys. J.* **2002**, *82*, 432A–432A.
(33) Pastor, I.; Ferrer, M. L.; Lillo, M. P.; Gomez, J.; Mateo, C. R. *J. Phys. Chem. B* **2007**, *111*, 11603–11610.

AM900430V